

Scattering of Goldstone Bosons and resonance production in a Composite Higgs model on the lattice

Vincent Drach^a Tadeusz Janowski^b Claudio Pica^c Sasa Prelovsek^{d,e,f}

^aCentre for Mathematical Sciences, Plymouth University, Plymouth, PL4 8AA, United Kingdom

^bSchool of Physics and Astronomy, University of Edinburgh, Edinburgh EH9 3FD, United Kingdom

^cCP3-Origins and eScience Center, University of Southern Denmark, Campusvej 55, DK-5230 Odense M, Denmark

^dFaculty of Mathematics and Physics, University of Ljubljana, Slovenia

^eJozef Stefan Institute, Ljubljana, Slovenia

^fInstitute for Theoretical Physics, University of Regensburg, Germany

E-mail: vincent.drach@plymouth.ac.uk, pica@cp3-origins.net,
sasa.prelovsek@ijs.si

ABSTRACT: We calculate the coupling between a vector resonance and two Goldstone bosons in $SU(2)$ gauge theory with $N_f = 2$ Dirac fermions in the fundamental representation. The considered theory can be used to construct a minimal Composite Higgs models. The coupling is related to the width of the vector resonance and we determine it by simulating the scattering of two Goldstone bosons where the resonance is produced. The resulting coupling is $g_{VPP} = 7.8 \pm 0.6$, not far from $g_{\rho\pi\pi} \simeq 6$ in QCD. This is the first lattice calculation of the resonance properties for a minimal UV completion. This coupling controls the production cross section of the lightest expected resonance at the LHC and enters into other tests of the Standard Model, from Vector Boson Fusion to electroweak precision tests. Our prediction is crucial to constrain the model using lattice input and for understanding the behavior of the vector meson production cross section as a function of the underlying gauge theory. We also extract the coupling $g_{VPP}^{\text{KSRF}} = 9.4 \pm 0.6$ assuming the vector-dominance and find that this phenomenological estimate slightly overestimates the value of the coupling.

Contents

1	Introduction	1
2	Lattice setup	3
3	Vector resonance from scattering of two pseudoscalars	5
3.1	Goldstone Bosons scattering: flavour structure	6
3.2	Operators and correlators	7
3.3	Eigen-energies	7
3.4	Scattering amplitude and phase shift	8
3.5	Mass m_R , width Γ and the coupling g_{VPP} of the vector resonance	9
3.6	Comparison of the coupling g_{VPP} with the KSRF relation	11
4	Conclusions	11
A	Conventions	13

1 Introduction

Among the numerous approaches to address the shortcomings of the Standard Model, new strongly coupled sectors provide a number of interesting mechanisms that address fundamental issues like the naturalness problem or the origin of the Higgs' field.

Pseudo Nambu-Goldstone Boson (PNGB) Composite Higgs models aim at identifying the Higgs degrees of freedom with the Goldstone bosons of a new strongly coupled sector [1–3]. In this framework, the fundamental Higgs field of the Standard Model is an effective low energy degree of freedom at the electroweak scale of a new strongly interacting sector featuring spontaneous chiral symmetry breaking. The mechanism alleviates the naturalness problem. The coupling of the new strongly interaction sector with the Standard Model breaks explicitly the flavour symmetry of the underlying gauge theory. This breaking is responsible for a non-trivial potential for the pseudo-Goldstone bosons which provides the Higgs with a mass and triggers electroweak symmetry breaking.

These models are constrained by comparing predictions at the electroweak scale with the LHC data. Typically the predictions depends on low energy constants (LECs) of the effective theory and on free parameters that are related to the model building itself. The vast majority of models are tested without specifying an underlying strongly interacting sector, and by assuming that the LECs are free parameters. While the approach allows to investigate entire classes of UV completion, it neglects correlations among LECs and additional information provided by a quantitative understanding of the strong dynamics. The

lattice approach allows to make first-principle predictions of the low energy parameters and can therefore provide stringent constraints on some scenarios.

Strongly interacting theories are expected to feature a rich spectrum of resonances that modify the phenomenology at colliders. In minimal scenarios, vector resonance are expected to mix with the electroweak bosons and can therefore be produced via vector boson fusion or via the Drell-Yan production mechanism, see for instance [4, 5]. These processes are controlled by the coupling g_{VPP} of the vector resonance (V) to two pseudoscalar Goldstone bosons (P). The phenomenology of new vector resonances is attracting considerable attention by the community [6–12].

In this work, we perform the first ab-initio calculation of the coupling g_{VPP} between a resonance and a pair of Goldstone bosons using lattice techniques in isolation of the Standard Model for a minimal UV completion. We consider $SU(2)$ gauge theory with $N_f = 2$ fundamental Dirac fermions. The theory features an extended $SU(4)$ flavour symmetry that spontaneously breaks to $Sp(4)$. It is used to build a PNCB Composite Higgs models in [13] and was recently reviewed in [14]. In this model the physical Higgs boson is a mixture of PNCBs and of the scalar state of the strong sector. The phenomenology of the model has been shown to be viable in view of the LHC data in [15], and the mixing between the scalar resonance and the Higgs can relax the bounds on the model [9]. The phenomenology of vector resonances for theories sharing the same chiral symmetry breaking pattern is investigated in detail as a function vector meson coupling constant in [16]. The authors derived the bound from di-lepton and di-boson searches at the LHC, as well as the dependence of the electroweak precision parameters as a function of the coupling constant. Our work can therefore be used to constrain a minimal model more efficiently.

We determine the $V \rightarrow PP$ coupling by extracting the scattering amplitude for $PP \rightarrow V \rightarrow PP$ scattering in the vector channel via the rigorous Lüscher formalism [17, 18]. We apply techniques that have been widely used for $\pi\pi \rightarrow \rho \rightarrow \pi\pi$ scattering in QCD, for example [19–25]. The coupling g_{VPP} is inferred from a Breit Wigner parametrization of the scattering amplitude. This work represents the first fully-fledged scattering calculation of the coupling g_{VPP} in a 4D gauge theory with fermions beyond QCD. It complements previous studies addressing the phenomenology of models based on the same underlying gauge theory [26–31].

The coupling g_{VPP} was previously estimated via the phenomenological relation $g_{VPP}^{\text{KSRF}} = m_V/F_{PS}$ by Kawarabayashi-Suzuki-Riazuddin-Fayyazuddin (KSRF) [32, 33] that assumes the vector-meson dominance. These calculations were based on simulations where the vector state was stable. It was employed for QCD-like theories based on $SU(3)$ [34, 35] as well as various groups SU and Sp [35–39]. We refer to [34] for a discussion of the estimation of g_{VPP}^{KSRF} for a number of gauge theories. This relation turns out to be satisfied in QCD but has however never been rigorously tested beyond before this work. It is therefore crucial to guide model builders and searches for Beyond the Standard Model Physics.

2 Lattice setup

In the numerical simulations of $SU(2)$ gauge theory with $N_f = 2$, we choose a clover-improved Wilson action for the two flavours of Dirac fermions [40, 41] and the tree-level Symanzik improved action for the gauge sector [42]:

$$S = -\frac{\beta}{2} \sum_{x,\mu,\nu} c_0 \text{ReTr} P_{\mu\nu}(x) + c_1 \text{ReTr} (R_{\mu\nu}(x) + R_{\nu\mu}(x)) \quad (2.1)$$

$$+ \sum_{x,\mu} \bar{\psi}(x) (am_0 + 4) \psi(x) - \frac{1}{2} \bar{\psi}(x + \mu) U_\mu (1 - \gamma^\mu) \psi(x) + \frac{c_{sw}}{2} \sum_{x,\mu < \nu} \bar{\psi}(x) \sigma_{\mu\nu} \hat{F}^{\mu\nu} \psi(x).$$

Here U_μ is the gauge field, ψ is the doublet of u and d fermions, $P_{\mu\nu}$ is the plaquette, $R_{\mu\nu}$ is a 2×1 rectangular loop, $\hat{F}_{\mu\nu}$ is the Wilson clover term and β is the inverse lattice gauge coupling. The coefficient of the gauge action are set to $c_0 = 5/3$ and $c_0 + 8c_1 = 1$ [42]. The improvement coefficient $c_{SW} = 1$ is set to its tree-level value in our simulations. The presence of bare mass term am_0 and the Wilson term explicitly breaks the $SU(4)$ flavour symmetry to a $Sp(4)$ subgroup. We use periodic boundary conditions in all four directions for the fermions.

The results presented in this work are obtained at $\beta = 1.45$. For each ensemble, we compute the pseudoscalar meson mass m_{PS} , and vector meson mass m_V by fitting at large euclidean time the effective mass of appropriate two-points correlation function. We also determine the bare quark mass m_{PCAC} defined through the Partially Conserved Axial Current relation and the bare pseudoscalar decay constant F_{PS}^{bare} , which renormalizes multiplicatively with the renormalization factor Z_A . The normalization of F_{PS} corresponds to the convention where the pion decay constant in QCD is 130 MeV. More details concerning our calculation of these quantities can be found in [26] where we use the same strategy and normalization.

To compare our results with our previous results we convert the lattice quantities in physical units by setting the scale using the Wilson Flow observable w_0 [43]. The scale w_0 is defined by $W(w_0^2) = W_{\text{ref}}$ where $W(t) = t \frac{d}{dt} [t^2 E(t)]$ and $E(t)$ ¹ is the flowed action density at flow time t . The reference value W_{ref} is dimensionless and set to 1.0, consistently with our previous definition. The value of w_0/a is determined for a range of fermion masses and chirally extrapolated using NNLO expansion in terms of m_{PS}^2 [44]. We employ ensembles with $m_{PS}L > 4$, where the finite volume effects are small. The data and are shown in Fig. 1, together with the best fitting curve, and the 1σ error band in gray. The final results reads w_0^x/a ($\beta=1.45$) = 3.08(2) using the NNLO fit which has a $\chi^2/ndof = 6.5/4$.

In order to compare our result with the KSRF relation $g_{VPP} = m_V/F_{PS}$, it is necessary to renormalize the pseudoscalar decay constant with Z_A . We performed the non perturbative determination of Z_A in the RI'-MOM scheme [45], using the same strategy as in our previous setup [26]. The correlators are estimated using momentum sources introduced in [46]. To interpolate between the lattice momenta we furthermore use twisted boundary

¹ E and t are not to be confused with energy and Euclidian time employed later on.

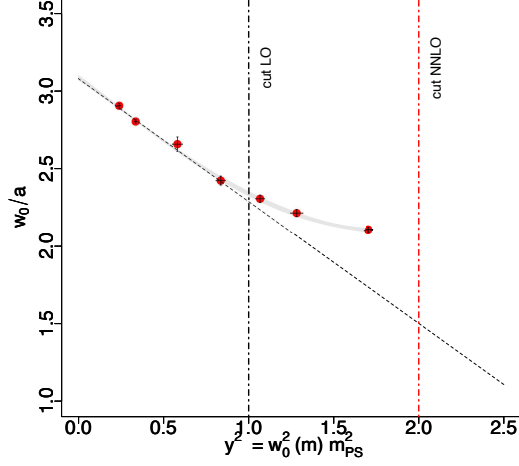


Figure 1. Chiral extrapolation of w_0/a as a function of $y^2 = w_0(m)^2 m_{PS}^2$. The lattice data are in red. The LO fit is represented by a dotted straight line and the NNLO fit is represented by a shaded gray area. The vertical dotted line denotes the maximal value of y^2 included in the LO and NNLO fits.

conditions [47, 48]. The amputated vertex function is then defined as follows:

$$\Pi_\mu(p) = S(p)^{-1} \left(\sum_{x,y,z} e^{-ip(x-z)} e^{-ip(z-y)} \langle \psi(x) \bar{\psi}(z) \gamma_\mu \gamma_5 \psi(z) \bar{\psi}(y) \rangle \right) S(p)^{-1}, \quad (2.2)$$

where $S^{-1}(p)$ is the inverse propagator in spin and color space. Defining,

$$\Lambda_A(p^2) = -i \frac{\text{tr} \left[\frac{\gamma_\mu \sin(ap_\mu)}{\sin^2(ap_\mu)} S^{-1}(p) \right]}{\sum_\mu \text{tr} [P_\mu \Pi_\mu(p)]}, \quad \text{with } P_\mu = \frac{\gamma_\mu \gamma_5}{4}, \quad (2.3)$$

it can be shown that in the chiral limit $\Lambda_A(p^2 = \mu^2) \rightarrow Z_A(\beta, \mu^2)$. The chiral extrapolation at fixed p^2 is performed using linear extrapolation in m_{PCAC} and our estimate of $\Lambda_A(p^2)$ in the chiral limit is shown in Fig. 2. We used $(w_0^x p)^2 = 7 > (w_0^x m_V)^2 \sim 1$ as a reference scale and our final estimate reads $Z_A(\beta = 1.45, (w_0^x p)^2 = 7) = 0.8022(3)$. The statistical errors are estimated using bootstrap resampling.

A range of simulations performed at $\beta = 1.45$ allowed us to determine simulation parameters so that $m_V > 2m_{PS}$, therefore allowing the decay of the vector meson into two Goldstone bosons. We used a single bare mass $m_0 = -0.6050$ to perform the calculation of the phase-shift of the two Goldstone boson scattering process, and two lattice volumes of $16^3 \times 32$ and $24^3 \times 48$. The value of the m_{PS} , m_{PCAC} and m_V^{naive} are summarized in Table 1. The topological charge was monitored during the runs, our simulations explore a range of topological sectors. In average the topological charge is compatible with zero. The scattering study employs the quark propagators that are combined from the propagators with periodic and anti-periodic boundary conditions in time in order to effectively double the time extent of the lattice, as detailed for example in [22].

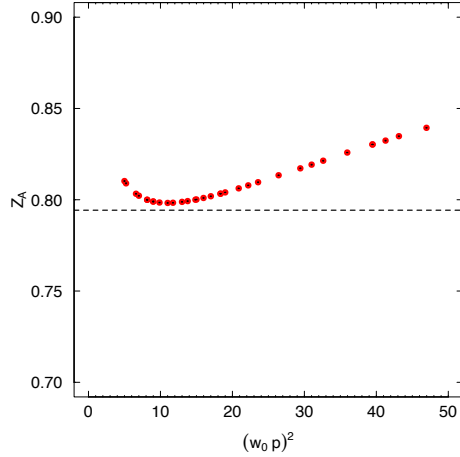


Figure 2. Behaviour of Z_A as a function of $(w_0 p)^2$ after the chiral extrapolation of Λ_A . The statistical errors are included. The perturbative value derived for the plaquette action and unimproved Wilson fermions [49] is shown by a black dashed line.

β	m_0	V	Stat.	$m_{\text{PS}}L$	am_{PCAC}	am_{PS}	$aF_{\text{PS}}^{\text{bare}}$	am_V^{naive}
1.45	-0.605	$16^3 \times 32$	1354	3.6	0.0107(7)	0.226(4)	0.048(2)	0.488(42)
1.45	-0.605	$24^3 \times 48$	1857	4.9	0.0107(2)	0.205(2)	0.058(1)	0.438(26)

Table 1. The main parameters of two lattice ensembles employed for the study of the vector resonance. The values obtained for am_{PCAC} , am_{PS} , aF_{PS} and am_V^{naive} are also provided.

3 Vector resonance from scattering of two pseudoscalars

The vector resonance V can decay into two pseudoscalar mesons P as shown based on the symmetries in the next subsection. The vector meson mass extracted from the two-point correlator on the chosen gauge ensemble is above the decay threshold $2m_{\text{PS}}$ and the decay is therefore kinematically allowed. A resonance is not an eigenstate of the Hamiltonian and its properties have to be inferred from the study of the scattering process $PP \rightarrow V \rightarrow PP$. We will show that the investigation of this resonance has similarities with the study of the ρ -vector resonance in QCD which has been studied through $\pi\pi \rightarrow \rho \rightarrow \pi\pi$ in numerous lattice QCD investigations, for example [19–25]. The main strategy is briefly reviewed here. The discrete eigen-energies E_n of two pseudoscalars in the finite box of size L and with periodic boundary conditions in space are determined. These are different from the non-interacting energies $E^{n,i} = (m_{\text{PS}}^2 + \mathbf{p}_1^2)^{1/2} + (m_{\text{PS}}^2 + \mathbf{p}_2^2)^{1/2}$ of two pseudoscalars with momenta $\mathbf{p}_{1,2} = \frac{2\pi}{L}\mathbf{n}_{1,2}$ due to mutual interactions of pseudoscalars. The energy-shifts $\Delta E = E_n - E^{n,i}$ give information on their interactions and therefore phase-shift in partial wave l . Lüscher’s formalism provides a rigorous relation between the eigen-energy E_{CM} of two-particles in a finite box and their infinite-volume scattering amplitude $S_l(E_{CM}) = e^{2i\delta_l(E_{CM})}$ at this energy E_{CM} in center-of-momentum frame [17, 50]. We will extract the phase shift for seven values of energy by considering the lowest two eigenstates $E_{n=1,2}$ in two different inertial

frames and two different volumes². The energy-dependence of the phase shift will have a resonance shape. The resonance mass, width and the $V \rightarrow PP$ coupling g_{VPP} will be extracted from this dependence via the Breit-Wigner type fit.

3.1 Goldstone Bosons scattering: flavour structure

We consider the scattering channels of the two-Goldstone boson scattering in $SU(2)$ gauge theory with $N_f = 2$ fundamental fermions. The goal of this section is to show that one can employ the interpolators with the flavor structure analogous to QCD. For this purpose we demonstrate that the operators $\pi^- \pi^+ - \pi^+ \pi^-$ and ρ_μ belong to the ten-dimensional irreducible representation of $Sp(4)$, where π and ρ are bilinears

$$\pi^+ = -\bar{d}\gamma_5 u, \quad \pi^- = \bar{u}\gamma_5 d, \quad \rho_\mu = \bar{u}\gamma_\mu u - \bar{d}\gamma_\mu d. \quad (3.1)$$

We follow the convention used for instance in [51] and summarized in appendix A, where

$$Q = \begin{pmatrix} u_L \\ d_L \\ \tilde{u}_L \\ \tilde{d}_L \end{pmatrix} = \begin{pmatrix} u_L \\ d_L \\ (-i\sigma_2)C\bar{u}_R^T \\ (-i\sigma_2)C\bar{d}_R^T \end{pmatrix}, \quad E = \begin{pmatrix} 0 & \mathbb{1}_2 \\ -\mathbb{1}_2 & 0 \end{pmatrix}, \quad (3.2)$$

the Pauli matrix acts in colour space and $C = i\gamma_0\gamma_2$ is the conjugation charge matrix. It can be shown that the massless Lagrangian is symmetric under $SU(4)$ transformation, while the mass term can be shown to be $Sp(4)$ invariant.

Let's focus on the multiplet $\Pi^{i=1,\dots,5}$ and the decoupled $V_\mu^{a=1,\dots,10}$ defined as

$$\Pi^i = Q^T(-i\sigma_2)C\gamma_5 X^i EQ + \left(Q^T(-i\sigma_2)C\gamma_5 X^i EQ\right)^\dagger, \quad V_\mu^a = \bar{Q}S^a\gamma_\mu Q. \quad (3.3)$$

Here $X^{i=1,\dots,5}$ are the broken generators used to parametrized the coset $SU(4)/Sp(4)$, while $S^{a=1,\dots,10}$ are the generators of $Sp(4)$ defined in the appendix.

Consider an infinitesimal the infinitesimal transformation $Q \rightarrow (\mathbb{1}_4 + i\alpha^a S^a)Q$ where $\alpha^{i=1,\dots,10}$ are real parameters. The explicit calculation shows that the multiplet Π transforms as $\Pi \rightarrow \Pi + G\Pi$, where $G = 2i\sqrt{2}\alpha^a T^a$ is a skew-symmetric matrix which can be written as a linear combination of the generators $T^{a=1,\dots,10}$ of $SO(5)$ defined in the appendix. The multiplet Π therefore transforms as a 5-dimensional irreducible representation of $Sp(4)$.

The transformation of the tensor product of two Goldstone Bosons operators $\Pi \otimes \Pi$ can then be worked out. In this work, we focus on the antisymmetric part of the tensor:

$$H^{ij} = \frac{1}{2} (\Pi^i \Pi^j - \Pi^j \Pi^i). \quad (3.4)$$

Defining the 10-dimensional vector $F^a = \text{tr}[T^a H]$, an explicit calculation shows that $F^a \rightarrow F^a + 2if_{abc}\alpha^b F^c$, where f_{abc} are the structure constant of $Sp(4)$. The multiplet $F^{a=1,\dots,10}$ therefore belongs to a 10-dimensional irreducible representation of $Sp(4)$. Furthermore, expressing

²This renders eight values of E_{CM} and $\delta(E_{CM})$, but one of them will have large uncertainty and will not be employed.

Eq. (3.3) in terms of the u and d fields via Eq. (3.2), using properties of the conjugation charge matrix and of the skew-symmetric matrix $(-i\sigma_2)$ acting in color space, we find that $F^3 = \frac{1}{4}(\pi^-\pi^+ - \pi^+\pi^-)$. In a similar manner the bilinears V_μ^a transform as $V^a \rightarrow V^a + if_{abc}\alpha^b S^c$ and $V_\mu^3 = \rho_\mu$.

In other words, we have shown that the usual 3-dimensional irrep ($I = 1$) of the isospin group is contained in the 10-dimensional representation of $Sp(4)$. Regarding discrete symmetries, it is straightforward to check that F^3 and ρ_μ have negative parity and negative charge conjugation.

3.2 Operators and correlators

The aim is to extract eigen-energies of the system with the quantum numbers of the vector resonance, namely $J^P = 1^-$. Given the flavour structure discussed in the previous section, we employ the two following operators:

$$\begin{aligned} O_{PP}(t, \mathbf{p}, \mathbf{0}) = O_1 &= \frac{1}{\sqrt{2}} \sum_{\mathbf{x}} \bar{d}(x) \gamma^5 u(x) e^{i\mathbf{p}\cdot\mathbf{x}} \sum_{\mathbf{y}} \bar{u}(y) \gamma^5 d(y) e^{i\mathbf{y}\cdot\mathbf{0}} - \{u \leftrightarrow d\} \propto P^+(\mathbf{p})P^-(0) - P^-(\mathbf{p})P^+(0) \\ O_V(t, \mathbf{p}) = O_2 &= \frac{1}{\sqrt{2}} \sum_{\mathbf{x}} \bar{u}(x) (\gamma \cdot \frac{\mathbf{p}}{|\mathbf{p}|}) u(x) e^{i\mathbf{p}\cdot\mathbf{x}} - \{u \leftrightarrow d\}. \end{aligned} \quad (3.5)$$

To compute the phase shift for different values of E_{CM} we consider two inertial frames with total momenta $\mathbf{P}_{tot} = \mathbf{p} = (0, 0, 1)$ and $(1, 1, 0)$ in units of $2\pi/L$. The operators with momenta $(0, 0, 1)$ transform according to the irreducible representation A_2^- of the group D_{4h} within the notation of [18]. The operators with momenta $(1, 1, 0)$ transform according to B_1^- of the group D_{2h} in the notation of [21].

The eigen-energies are obtained by computing in each frame the 2×2 correlation matrix

$$C(t, \mathbf{p}) = \begin{pmatrix} \langle O_{PP}(t, \mathbf{p}, \mathbf{0}) O_{PP}^\dagger(0, \mathbf{p}, \mathbf{0}) \rangle & \langle O_{PP}(t, \mathbf{p}, \mathbf{0}) O_V^\dagger(0, \mathbf{p}) \rangle \\ \langle O_V(t, \mathbf{p}) O_{PP}^\dagger(0, \mathbf{p}, \mathbf{0}) \rangle & \langle O_V(t, \mathbf{p}) O_V^\dagger(0, \mathbf{p}, \mathbf{0}) \rangle \end{pmatrix}, \quad (3.6)$$

which renders the Wick contractions analogous to those in QCD. We evaluate those with the stochastic $U(1)$ noise technique used in simulations [19, 20] of ρ -meson decay in QCD.

The experience from analogous studies of $\pi\pi \rightarrow \rho \rightarrow \pi\pi$ scattering in QCD indicates that it is crucial to employ one $\bar{q}q$ operator and the $\pi\pi$ operators relevant in the given energy range to obtain eigen-energies of the system. Adding more $\bar{q}q$ operators with given quantum numbers does not affect the eigen-energies, as illustrated for example in Fig. 8 of [22]. Therefore we expect that two employed operators suffice to extract eigen-energies in this energy range.

3.3 Eigen-energies

The time-dependence of the correlation matrix $C_{ij}(t) = \langle 0 | O_i(t) O_j^\dagger(0) | 0 \rangle = \sum_n \langle 0 | O_i | n \rangle e^{-E_n t} \langle n | O_j^\dagger | 0 \rangle$ contains information on the eigen-energies E_n . We extract those using the widely used GEVP variational method [52–54]

$$C(t)u^{(n)}(t) = \lambda_n(t)C(t_0)u^{(n)}(t_0), \quad \lambda_n(t) \xrightarrow{\text{large } t} A_n e^{-E_n t} \quad (3.7)$$

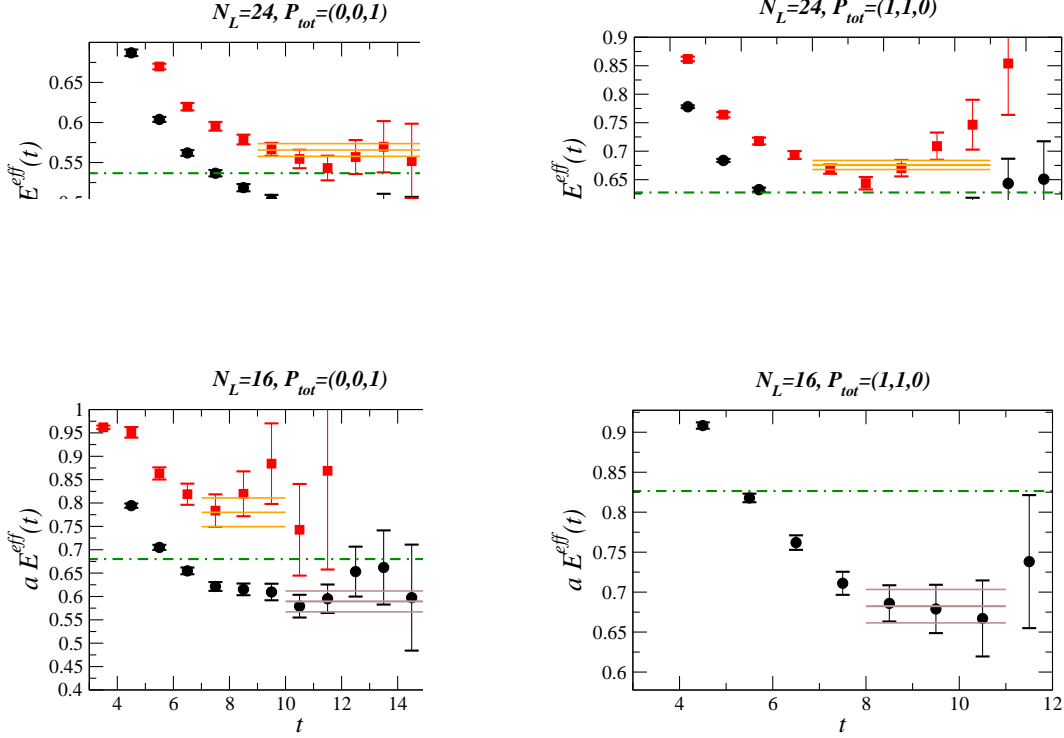


Figure 3. The effective energies $E_n^{eff}(t)$ for seven eigenstates of the two-pseudoscalar system on a finite lattice. The fitted eigen-energies E_n are also provided together with the fit-ranges (3.7). The dot-dashed lines indicate non-interacting energy $E^{n.i.} = (m_{\text{PS}}^2 + \mathbf{p}^2)^{1/2} + m_{\text{PS}}$ of two -pseudoscalar system $P(0)P(\mathbf{p})$.

with reference time $t_0 = 4$.

The effective energies $E_n^{eff}(t) = \log[\lambda_n(t)/\lambda_n(t+1)]$ for seven eigenstates are given in Fig. 3 and they are related to E_n in the plateau region. They correspond to lowest two eigenstates for two inertial frames and two volumes; the first excited state for $N_L = 16$ and $\mathbf{P}_{tot} = (1, 1, 0)$ has a large statistical uncertainty and will not be used in analysis. We do not find an indication for non-exponential time-dependence at large t before the signal is lost in the noise since the size of the time-direction has been effectively doubled by combining periodic and antiperiodic propagators in time. The eigen-energies E_n are extracted from the correlated one-exponential fits (3.7) of eigenvalues $\lambda_n(t)$ in the plateau region, that are indicated in the Fig. 3 and tabulated in 2.

3.4 Scattering amplitude and phase shift

The eigen-energies E_n in Fig. 3 (solid lines) are shifted with respect to non-interacting energy $E^{n.i.} = (m_{\text{PS}}^2 + \mathbf{p}^2)^{1/2} + m_{\text{PS}}$ of two-pseudoscalar system $P(\mathbf{p})P(0)$ (dot-dashed lines). These non-zero shifts are essential for extracting the scattering information.

The relation between eigen-energy E_{CM} of two particles and infinite-volume scattering phase shift $\delta(E_{CM})$ at that energy was derived by Lüscher [17] for $\mathbf{P}_{tot} = 0$. This relation was generalized in [18, 21] for inertial frames with $\mathbf{P}_{tot} = (0, 0, 1)$ and $(1, 1, 0)$ that are

N_L	\mathbf{P}_{tot}	level n	fit-range	$E_n a$	$E_{CM} a$	$(\frac{p_* L}{2\pi})^2$	$\frac{(p_* a)^3 \cot \delta_1}{E_{CM} a}$	$\delta_{l=1} [^\circ]$
24	(0,0,1)	1	10-17	0.491(7)	0.415(8)	0.016(23)	0.0055(11)	0.9(1.4)
24	(0,0,1)	2	9-15	0.566(8)	0.501(9)	0.30(3)	-0.027(5)	167(4)
24	(1,1,0)	1	8-13	0.575(6)	0.440(8)	0.093(27)	0.0045(11)	14.3(2.2)
24	(1,1,0)	2	8-13	0.676(8)	0.565(9)	0.55(4)	-0.025(3)	152(4.9)
16	(0,0,1)	1	10-15	0.589(22)	0.440(30)	-0.020(42)	0.013(3)	-1.7(5.8)i
16	(0,0,1)	2	7-10	0.780(31)	0.674(36)	0.40(8)	-0.044(8)	152(10)
16	(1,1,0)	1	8-11	0.682(21)	0.397(36)	-0.078(46)	0.0085(17)	-24(20)i

Table 2. Seven eigen-states of PP system and the resulting information related to the scattering phase shift δ_l for partial-wave $l = 1$.

employed here. In this case, the eigenstate with energy E_n corresponds to the energy $E_{CM} = (E_n^2 - \mathbf{P}_{tot}^2)^{1/2}$ in the center-of-momentum frame, where pseudoscalars $P(\mathbf{p}_*)P(-\mathbf{p}_*)$ have back-to-back momenta $p_* = (E_{CM}^2/4 - m_{PS}^2)^{1/2}$ and dimension-less momenta $q = p_* L/(2\pi)$. The relation between eigen-energy (or corresponding q) and the scattering phase-shift at that energy (or q) is given by

$$\tan \delta_1(q) = \frac{\pi^{3/2} q \gamma}{Z_{00}(1; q^2) + \frac{2}{\sqrt{5} q^2} Z_{20}(1; q^2)} \quad \text{for } \mathbf{P}_{tot} = (0, 0, 1) \quad (3.8)$$

$$\tan \delta_1(q) = \frac{\pi^{3/2} q \gamma}{Z_{00}(1; q^2) - \frac{1}{\sqrt{5} q^2} Z_{20}(1; q^2) - i \frac{\sqrt{3}}{\sqrt{10} q^2} (Z_{22}(1; q^2) - Z_{2(-2)}(1; q^2))} \quad \text{for } \mathbf{P}_{tot} = (1, 1, 0),$$

for the relevant irreducible representations of the symmetry groups listed after Eq. (3.5). Here δ_1 denotes phase shift for partial-wave $l = 1$, $Z_{lm}(s, q^2) = \sum_{n \in P_d} Y_{lm}(n)/(q^2 - n^2)^s$ [21] and $\gamma = (1 - v^2)^{-1/2}$.

Every eigen-energy E_n renders certain E_{CM} , q and phase shift, which are tabulated for seven eigenstates in Table 2. The dependence of the phase-shift on E_{CM} is plotted in Fig. 4a. It increases from the small values, past the resonance value 90° to the large values.

3.5 Mass m_R , width Γ and the coupling g_{VPP} of the vector resonance

The energy dependence of the phase shift for PP scattering in Fig. 4a shows a behavior expected for a narrow resonance that lies slightly above threshold: it rises from small values, through the resonance value 90° at about $m_{Ra} = E_{CM} a \simeq 0.45$, to the large values close to 180° . It is expected to have a Breit-Wigner type resonance form in the vicinity of a narrow vector resonance

$$\tan \delta_1(E_{CM}) = \frac{E_{CM} \Gamma(E_{CM})}{m_R^2 - E_{CM}^2}, \quad \Gamma(E_{CM}) = \frac{g_{VPP}^2 p_*^3}{6\pi E_{CM}^2}. \quad (3.9)$$

The resonance width $\Gamma(E_{CM})$ is parametrized in terms of the $V \rightarrow PP$ coupling g_{VPP} and the phase space for partial wave $l = 1$, where p_* is the momentum of the pseudoscalar in

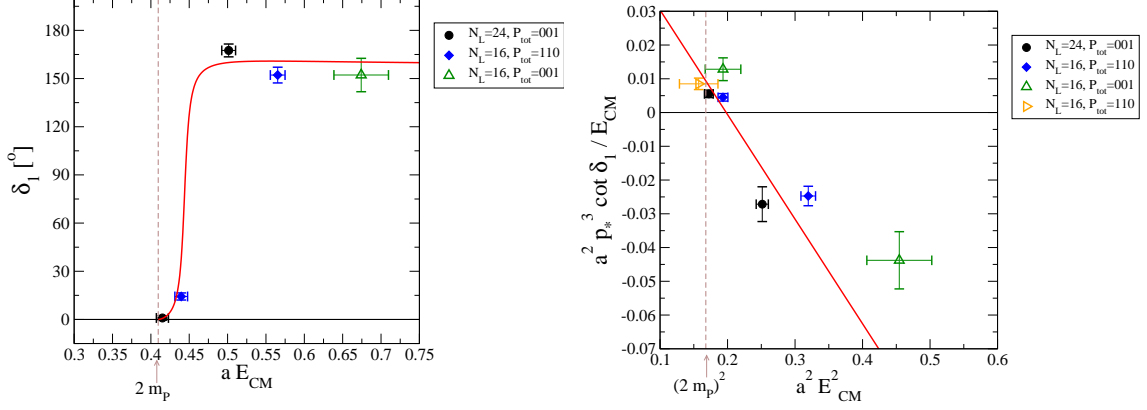


Figure 4. Results on the scattering PP of two pseudoscalars in partial-wave $l=1$. (a) Scattering phase-shift δ_1 as a function of center-of-momentum energy E_{CM} . (b) Quantity $p_*^3 \cot \delta_1(E_{CM})/E_{CM}$ as a function of E_{CM}^2 , which is expected to be linear in case of Breit-Wigner resonance. The red solid line shows the Breit-Wigner resonance fit (3.9,3.10) with the values of resonance parameters (3.12). Dashed vertical line indicates the position of the threshold for $N_L = 24$. The left plot omits the points below threshold that lead to imaginary phase shifts.

CM frame. The resonance phase shift (3.9) implies that $p_*^3 \cot \delta_1/E_{CM}$ is a linear function of E_{CM}^2

$$\frac{p_*^3 \cot \delta_1(E_{CM})}{E_{CM}} = \frac{6\pi}{g_{VPP}^2} (m_R^2 - E_{CM}^2). \quad (3.10)$$

This quantity is shown in Fig. 4b for PP scattering from our lattice simulation. It is falling with energy, it crosses through the resonance value $\cot \delta_1 = 0$ at $E_{CM} = m_R$ and roughly supports the linear dependence on E_{CM}^2 .

Finally, we proceed to determine the vector resonance parameters from the phase shift that shows a resonant shape. We aim to determine the mass m_R and the coupling g_{VPP} that parametrizes the width rather than the width itself. The width is strongly dependent on m_{PS} through the phase space, while the dependence of g_{VPP} on m_{PS} is expected to be much milder (the dependence of $g_{\rho\pi\pi}$ on m_π in QCD is very mild as evidenced in the review of various lattice results [24, 25]). The m_R and g_{VPP} can be read-off from zero and the slope for the quantity (3.10) in Fig. 4b. In order to take the correlations properly into account, we extract m_R and g_{VPP} by minimizing the correlated χ^2

$$\chi^2 = \sum_{k=1}^{N_k} \sum_{k'=1}^{N_k} [E_k - E_k^{par}(m_R, g_{VPP})] \text{Cov}^{-1}(k, k') [E_{k'} - E_{k'}^{par}(m_R, g_{VPP})] \quad (3.11)$$

with $N_k = 7$ for seven eigenstates. Here $E_{k=1, \dots, N_k}$ are energies of seven eigenstates determined on the lattice. $\text{Cov}(k, k')$ is their 7×7 covariance matrix, where $\text{Cov}(k, k') = 0$ if eigenstates k and k' correspond to ensembles with different N_L . The $E_k^{par}(m_R, g_{VPP})$ is the value of E_k determined analytically for given m_R and g_{VPP} based on the parametrization (3.10) and δ_1 from Lüscher-type relation (3.8).

The final parameters of the vector resonance based on minimization of χ^2 (3.11) are

$$m_{Ra} = 0.445 \pm 0.008 \pm 0.002 \quad g_{VPP} = 7.8 \pm 0.5 \pm 0.1$$

$$\text{with } \text{cor}(m_R, g_{VPP}) = 0.35 \quad \text{and} \quad \chi^2/\text{dof} = 1.5 . \quad (3.12)$$

The first error is statistical and arises from the errors on the energies encoded in the covariance matrix, while the second error accounts for the uncertainty in the pseudoscalar mass.

The correlation between resonance parameters is provided by $\text{cor} = \frac{\langle(g-\langle g \rangle)(m_R-\langle m_R \rangle)\rangle}{\sqrt{\langle(g-\langle g \rangle)^2}\sqrt{\langle(m_R-\langle m_R \rangle)^2}}$.

The phase-shift dependence based on these resonance parameters (3.12) is plotted by red solid lines in Fig. 4. The results (3.12) are based on seven eigenstates from both volumes $N_L = 24, 16$. Restricting the fit to four eigenstates on the larger volume $N_L = 24$, one gets compatible results $m_{Ra} = 0.442 \pm 0.009 \pm 0.002$, $g_{VPP} = 7.7 \pm 0.5 \pm 0.1$ with $\text{cor} = 0.37$ and $\chi^2/\text{dof} = 1.7$. For comparison, Table 1 presents the mass of a vector particle (am_V^{naive}) obtained using a single $\bar{q}q$ operator in a conventional way.

Note that the calculation is performed at the finite pseudoscalar meson mass and at finite lattice spacing. However it should be noted that lattice results on $g_{\rho\pi\pi}$ in QCD do not show large discretization errors and that its dependence on m_π is very mild: the compilation [24, 25] of lattice simulations by several groups shows that the coupling is $g_{\rho\pi\pi} \simeq 6$ for a wide range of m_π and lattice spacings. We therefore believe our calculation provides a first estimate of the coupling g_{VPP} in the chiral limit of $SU(2)$ gauge theory with two fundamental flavors of Dirac fermions.

3.6 Comparison of the coupling g_{VPP} with the KSRF relation

The $V \rightarrow PP$ coupling is often determined phenomenologically via the KSRF relation $g_{VPP}^{\text{KSRF}} = m_V/F_{PS}$ based on the vector-meson dominance [32, 33]. This relation gives us

$$g_{VPP}^{\text{KSRF}} = m_V^{\text{naive}}/(Z_A F_{PS}^{\text{bare}}) = 9.4(6) \quad (3.13)$$

at finite m_{PS} , $V = 24^3 \times 48$ and Z_A provided in Section 2. The central value g_{VPP}^{KSRF} is 20% larger than the value g_{VPP} (3.12) rigorously extracted from the scattering.

Note furthermore that using our previous calculation with an unimproved action [26], and using the value of m_V and F_{PS} extrapolated to the chiral and continuum limit, we found $g_{VPP}^{\text{KSRF}} = 13.1(2.2)$. The value $g_{VPP}^{\text{KSRF}} = 15.6(4)$ used in [34] is from an update analysis including more gauge ensembles [55]. Our calculation therefore suggests that the KSRF relation overestimates the value of the coupling g_{VPP} for $SU(2)$ gauge theory with two fundamental flavors of Dirac fermions and that the control of systematics must be improved in order to clarify the overall picture as a function of the number of flavours.

4 Conclusions

We determined the coupling g_{VPP} between a vector resonance and a pair of Goldstone bosons in a minimal realization of a composite Higgs model. This is the first lattice result for the coupling of a decaying resonance in a such 4-dimensional gauge theories with

fermions. The calculation is performed by considering the scattering of two Goldstone bosons in the channel of the vector resonance. Assuming that the chiral dependence of g_{VPP} is mild (like in QCD) and that the discretization error are negligible, we obtain a rigorous estimate of the coupling in the continuum and in the chiral limit based on the non-perturbative calculation. The result suggests a rather large value of the coupling but smaller than the one obtained using the KSRF relation. Additional numerical simulations would be required to obtain a more definite answer. The coupling is relevant to constrain the phenomenology of a vector resonance in composite Higgs model at the LHC, and bring additional constraints on Vector Boson Scattering and on electroweak precision tests.

Acknowledgments

We would like to thank D. Buarque Franzosi, G. Cacciapaglia and F. Sannino for useful discussions at various stages of this project. The initial steps of this project have been performed on the HPC facilities at the HPCC centre of the University of Plymouth. This work was performed using the Cambridge Service for Data Driven Discovery (CSD3), part of which is operated by the University of Cambridge Research Computing on behalf of the STFC DiRAC HPC Facility (www.dirac.ac.uk). The DiRAC component of CSD3 was funded by BEIS capital funding via STFC capital grants ST/P002307/1 and ST/R002452/1 and STFC operations grant ST/R00689X/1. DiRAC is part of the National e-Infrastructure. S. P. was supported by Slovenian Research Agency ARRS (research core funding No. P1-0035 and No. J1-8137) and DFG grant No. SFB/TRR 55.

A Conventions

We follow the convention used in [51], where

$$\sigma_1 = \begin{pmatrix} 0 & 1 \\ 1 & 0 \end{pmatrix}, \quad \sigma_2 = \begin{pmatrix} 0 & -i \\ i & 0 \end{pmatrix}, \quad \sigma_3 = \begin{pmatrix} 1 & 0 \\ 0 & -1 \end{pmatrix}, \quad \sigma_4 = \begin{pmatrix} 1 & 0 \\ 0 & 1 \end{pmatrix}, \quad E = \begin{pmatrix} 0 & \sigma_4 \\ -\sigma_4 & 0 \end{pmatrix}$$

and

$$B_1 = \sigma_4, B_2 = i\sigma_4, B_3 = \sigma_3, B_4 = i\sigma_3, B_5 = \sigma_1, B_6 = i\sigma_1, \quad D_4 = \sigma_2, D_5 = i\sigma_2.$$

The fifteen generators of $SU(4)$ are denoted S^a and X^i with $a = 1, \dots, 10$ and $i = 1, \dots, 5$. The generators S^a satisfy the relation $(S^a)^T E + E S^a = 0$ and are a representation of $Sp(4)$:

$$S^a = \frac{1}{2\sqrt{2}} \begin{pmatrix} \sigma_i & 0 \\ 0 & -\sigma_i^T \end{pmatrix}, \quad a = 1, \dots, 4 \quad S^a = \frac{1}{2\sqrt{2}} \begin{pmatrix} 0 & B_i \\ B_i^\dagger & 0 \end{pmatrix}, \quad a = 5, \dots, 10$$

$$X^i = \frac{1}{2\sqrt{2}} \begin{pmatrix} \sigma_i & 0 \\ 0 & \sigma_i^T \end{pmatrix}, \quad i = 1, \dots, 3 \quad X^i = \frac{1}{2\sqrt{2}} \begin{pmatrix} 0 & D_i \\ D_i^\dagger & 0 \end{pmatrix}, \quad i = 4, 5.$$

The generators are normalized so that :

$$\text{tr}[S^a S^b] = \frac{1}{2} \delta^{ab}, \quad \text{tr}[X^i X^j] = \frac{1}{2} \delta^{ij}, \quad \text{tr}[S^a X^i] = 0.$$

The structure constant of the algebra of $Sp(4)$ are defined as $f_{abc} = 2\text{tr}[S^a[S^b, S^c]]$.

The 10 generators of $SO(5)$ with normalization $\text{Tr}[T^i T^j] = \frac{1}{2} \delta^{ij}$ are defined as follows:

$$T^1 = \frac{i}{2} \begin{pmatrix} 0 & 0 & 0 & 0 & 0 \\ 0 & 0 & 1 & 0 & 0 \\ 0 & -1 & 0 & 0 & 0 \\ 0 & 0 & 0 & 0 & 0 \\ 0 & 0 & 0 & 0 & 0 \end{pmatrix} \quad T^2 = \frac{i}{2} \begin{pmatrix} 0 & 0 & 1 & 0 & 0 \\ 0 & 0 & 0 & 0 & 0 \\ -1 & 0 & 0 & 0 & 0 \\ 0 & 0 & 0 & 0 & 0 \\ 0 & 0 & 0 & 0 & 0 \end{pmatrix} \quad T^3 = \frac{i}{2} \begin{pmatrix} 0 & 1 & 0 & 0 & 0 \\ -1 & 0 & 0 & 0 & 0 \\ 0 & 0 & 0 & 0 & 0 \\ 0 & 0 & 0 & 0 & 0 \\ 0 & 0 & 0 & 0 & 0 \end{pmatrix} \quad T^4 = \frac{i}{2} \begin{pmatrix} 0 & 0 & 0 & 0 & 0 \\ 0 & 0 & 0 & 0 & 0 \\ 0 & 0 & 0 & 0 & 0 \\ 0 & 0 & 0 & 0 & -1 \\ 0 & 0 & 0 & 1 & 0 \end{pmatrix}$$

$$T^5 = \frac{i}{2} \begin{pmatrix} 0 & 0 & 0 & 0 & 0 \\ 0 & 0 & 0 & 0 & 1 \\ 0 & 0 & 0 & 0 & 0 \\ 0 & 0 & 0 & 0 & 0 \\ 0 & -1 & 0 & 0 & 0 \end{pmatrix} \quad T^6 = \frac{i}{2} \begin{pmatrix} 0 & 0 & 0 & 0 & 0 \\ 0 & 0 & 0 & 1 & 0 \\ 0 & 0 & 0 & 0 & 0 \\ 0 & -1 & 0 & 0 & 0 \\ 0 & 0 & 0 & 0 & 0 \end{pmatrix} \quad T^7 = \frac{i}{2} \begin{pmatrix} 0 & 0 & 0 & 1 & 0 \\ 0 & 0 & 0 & 0 & 0 \\ 0 & 0 & 0 & 0 & 0 \\ -1 & 0 & 0 & 0 & 0 \\ 0 & 0 & 0 & 0 & 0 \end{pmatrix} \quad T^8 = \frac{i}{2} \begin{pmatrix} 0 & 0 & 0 & 0 & -1 \\ 0 & 0 & 0 & 0 & 0 \\ 0 & 0 & 0 & 0 & 0 \\ 0 & 0 & 0 & 0 & 0 \\ 1 & 0 & 0 & 0 & 0 \end{pmatrix}$$

$$T^9 = \frac{i}{2} \begin{pmatrix} 0 & 0 & 0 & 0 & 0 \\ 0 & 0 & 0 & 0 & 0 \\ 0 & 0 & 0 & -1 & 0 \\ 0 & 0 & 1 & 0 & 0 \\ 0 & 0 & 0 & 0 & 0 \end{pmatrix} \quad T^{10} = \frac{i}{2} \begin{pmatrix} 0 & 0 & 0 & 0 & 0 \\ 0 & 0 & 0 & 0 & 0 \\ 0 & 0 & 0 & 0 & 1 \\ 0 & 0 & 0 & 0 & 0 \\ 0 & 0 & -1 & 0 & 0 \end{pmatrix}. \quad (\text{A.1})$$

References

- [1] D.B. Kaplan and H. Georgi, *SU(2) x U(1) Breaking by Vacuum Misalignment*, *Phys. Lett. B* **136** (1984) 183.
- [2] D.B. Kaplan, H. Georgi and S. Dimopoulos, *Composite Higgs Scalars*, *Phys. Lett. B* **136** (1984) 187.
- [3] M.J. Dugan, H. Georgi and D.B. Kaplan, *Anatomy of a Composite Higgs Model*, *Nucl. Phys. B* **254** (1985) 299.
- [4] R. Contino and M. Salvarezza, *One-loop effects from spin-1 resonances in Composite Higgs models*, *JHEP* **07** (2015) 065 [[1504.02750](#)].
- [5] R. Contino, D. Marzocca, D. Pappadopulo and R. Rattazzi, *On the effect of resonances in composite Higgs phenomenology*, *JHEP* **10** (2011) 081 [[1109.1570](#)].
- [6] M. Gallinaro et al., *Beyond the Standard Model in Vector Boson Scattering Signatures*, 5, 2020 [[2005.09889](#)].
- [7] D. Liu, L.-T. Wang and K.-P. Xie, *Broad composite resonances and their signals at the LHC*, *Phys. Rev. D* **100** (2019) 075021 [[1901.01674](#)].
- [8] C. Helsens, D. Jamin, M.L. Mangano, T.G. Rizzo and M. Selvaggi, *Heavy resonances at energy-frontier hadron colliders*, *Eur. Phys. J. C* **79** (2019) 569 [[1902.11217](#)].
- [9] D. Buarque Franzosi, G. Cacciapaglia and A. Deandrea, *Sigma-assisted low scale composite Goldstone–Higgs*, *Eur. Phys. J. C* **80** (2020) 28 [[1809.09146](#)].
- [10] D. Liu, L.-T. Wang and K.-P. Xie, *Prospects of searching for composite resonances at the LHC and beyond*, *JHEP* **01** (2019) 157 [[1810.08954](#)].
- [11] D. Buarque Franzosi, *Implications of Vector Boson Scattering Unitarity in Composite Higgs Models*, *PoS EPS-HEP2017* (2017) 264.
- [12] D. Greco and D. Liu, *Hunting composite vector resonances at the LHC: naturalness facing data*, *JHEP* **12** (2014) 126 [[1410.2883](#)].
- [13] G. Cacciapaglia and F. Sannino, *Fundamental Composite (Goldstone) Higgs Dynamics*, *JHEP* **04** (2014) 111 [[1402.0233](#)].
- [14] G. Cacciapaglia, C. Pica and F. Sannino, *Fundamental Composite Dynamics: A Review*, *Phys. Rept.* **877** (2020) 1 [[2002.04914](#)].
- [15] A. Arbey, G. Cacciapaglia, H. Cai, A. Deandrea, S. Le Corre and F. Sannino, *Fundamental Composite Electroweak Dynamics: Status at the LHC*, *Phys. Rev. D* **95** (2017) 015028 [[1502.04718](#)].
- [16] D. Buarque Franzosi, G. Cacciapaglia, H. Cai, A. Deandrea and M. Frandsen, *Vector and Axial-vector resonances in composite models of the Higgs boson*, *JHEP* **11** (2016) 076 [[1605.01363](#)].
- [17] M. Luscher, *Two particle states on a torus and their relation to the scattering matrix*, *Nucl. Phys.* **B354** (1991) 531.
- [18] K. Rummukainen and S.A. Gottlieb, *Resonance scattering phase shifts on a nonrest frame lattice*, *Nucl. Phys.* **B450** (1995) 397 [[hep-lat/9503028](#)].
- [19] CP-PACS collaboration, *Lattice QCD Calculation of the rho Meson Decay Width*, *Phys. Rev.* **D76** (2007) 094506 [[0708.3705](#)].

- [20] CS collaboration, ρ Meson Decay in 2+1 Flavor Lattice QCD, *Phys. Rev.* **D84** (2011) 094505 [1106.5365].
- [21] X. Feng, K. Jansen and D.B. Renner, Resonance Parameters of the rho-Meson from Lattice QCD, *Phys. Rev.* **D83** (2011) 094505 [1011.5288].
- [22] C. Lang, D. Mohler, S. Prelovsek and M. Vidmar, Coupled channel analysis of the rho meson decay in lattice QCD, *Phys. Rev. D* **84** (2011) 054503 [1105.5636].
- [23] HADRON SPECTRUM collaboration, Energy dependence of the ρ resonance in $\pi\pi$ elastic scattering from lattice QCD, *Phys. Rev. D* **87** (2013) 034505 [1212.0830].
- [24] F. Erben, J.R. Green, D. Mohler and H. Wittig, Rho resonance, timelike pion form factor, and implications for lattice studies of the hadronic vacuum polarization, *Phys. Rev. D* **101** (2020) 054504 [1910.01083].
- [25] C. Alexandrou, L. Leskovec, S. Meinel, J. Negele, S. Paul, M. Petschlies et al., P -wave $\pi\pi$ scattering and the ρ resonance from lattice QCD, *Phys. Rev. D* **96** (2017) 034525 [1704.05439].
- [26] R. Arthur, V. Drach, M. Hansen, A. Hietanen, C. Pica and F. Sannino, $SU(2)$ gauge theory with two fundamental flavors: A minimal template for model building, *Phys. Rev. D* **94** (2016) 094507 [1602.06559].
- [27] R. Arthur, V. Drach, A. Hietanen, C. Pica and F. Sannino, $SU(2)$ Gauge Theory with Two Fundamental Flavours: Scalar and Pseudoscalar Spectrum, **1607.06654**.
- [28] R. Arthur, V. Drach, M. Hansen, A. Hietanen, C. Pica and F. Sannino, Scattering lengths in $SU(2)$ gauge theory with two fundamental fermions, *PoS LATTICE2014* (2014) 271 [1412.4771].
- [29] V. Drach, A. Hietanen, C. Pica, J. Rantaharju and F. Sannino, Template Composite Dark Matter : $SU(2)$ gauge theory with 2 fundamental flavours, in *Proceedings, 33rd International Symposium on Lattice Field Theory (Lattice 2015)*, 2015, <http://inspirehep.net/record/1404696/files/arXiv:1511.04370.pdf> [1511.04370].
- [30] A. Hietanen, R. Lewis, C. Pica and F. Sannino, Fundamental Composite Higgs Dynamics on the Lattice: $SU(2)$ with Two Flavors, *JHEP* **1407** (2014) 116 [1404.2794].
- [31] A. Hietanen, R. Lewis, C. Pica and F. Sannino, Composite Goldstone Dark Matter: Experimental Predictions from the Lattice, *JHEP* **12** (2014) 130 [1308.4130].
- [32] K. Kawarabayashi and M. Suzuki, Partially conserved axial vector current and the decays of vector mesons, *Phys. Rev. Lett.* **16** (1966) 255.
- [33] Riazuddin and Fayyazuddin, Algebra of current components and decay widths of rho and K^* mesons, *Phys. Rev.* **147** (1966) 1071.
- [34] D. Nogradi and L. Szikszai, The model dependence of m_ρ/f_π , in *37th International Symposium on Lattice Field Theory*, 2019 [1912.04114].
- [35] D. Nogradi and L. Szikszai, The flavor dependence of m_ρ/f_π , *JHEP* **05** (2019) 197 [1905.01909].
- [36] E. Bennett, D.K. Hong, J.-W. Lee, C.-J.D. Lin, B. Lucini, M. Mesiti et al., $Sp(4)$ gauge theories on the lattice: quenched fundamental and antisymmetric fermions, *Phys. Rev. D* **101** (2020) 074516 [1912.06505].
- [37] E. Bennett, D.K. Hong, J.-W. Lee, C.-J.D. Lin, B. Lucini, M. Piai et al., $Sp(4)$ gauge theories on the lattice: $N_f = 2$ dynamical fundamental fermions, *JHEP* **12** (2019) 053 [1909.12662].

- [38] V. Ayyar, T. DeGrand, M. Golterman, D.C. Hackett, W.I. Jay, E.T. Neil et al., *Spectroscopy of SU(4) composite Higgs theory with two distinct fermion representations*, *Phys. Rev. D* **97** (2018) 074505 [[1710.00806](#)].
- [39] LATTICE STRONG DYNAMICS collaboration, *Nonperturbative investigations of SU(3) gauge theory with eight dynamical flavors*, *Phys. Rev. D* **99** (2019) 014509 [[1807.08411](#)].
- [40] K.G. Wilson, *Confinement of Quarks*, .
- [41] B. Sheikholeslami and R. Wohlert, *Improved Continuum Limit Lattice Action for QCD with Wilson Fermions*, *Nucl. Phys. B* **259** (1985) 572.
- [42] M. Luscher and P. Weisz, *On-Shell Improved Lattice Gauge Theories*, *Commun. Math. Phys.* **97** (1985) 59.
- [43] S. Borsanyi et al., *High-precision scale setting in lattice QCD*, *JHEP* **09** (2012) 010 [[1203.4469](#)].
- [44] O. Bar and M. Golterman, *Chiral perturbation theory for gradient flow observables*, *Phys. Rev. D* **89** (2014) 034505 [[1312.4999](#)].
- [45] G. Martinelli, C. Pittori, C.T. Sachrajda, M. Testa and A. Vladikas, *A General method for nonperturbative renormalization of lattice operators*, *Nucl. Phys. B* **445** (1995) 81 [[hep-lat/9411010](#)].
- [46] M. Gockeler, R. Horsley, H. Oelrich, H. Perlt, D. Petters, P.E. Rakow et al., *Nonperturbative renormalization of composite operators in lattice QCD*, *Nucl. Phys. B* **544** (1999) 699 [[hep-lat/9807044](#)].
- [47] P.F. Bedaque, *Aharonov-Bohm effect and nucleon nucleon phase shifts on the lattice*, *Phys. Lett. B* **593** (2004) 82 [[nucl-th/0402051](#)].
- [48] C. Sachrajda and G. Villadoro, *Twisted boundary conditions in lattice simulations*, *Phys. Lett. B* **609** (2005) 73 [[hep-lat/0411033](#)].
- [49] L. Del Debbio, M.T. Frandsen, H. Panagopoulos and F. Sannino, *Higher representations on the lattice: Perturbative studies*, *JHEP* **06** (2008) 007 [[0802.0891](#)].
- [50] M. Luscher, *Signatures of unstable particles in finite volume*, *Nucl. Phys. B* **364** (1991) 237.
- [51] T.A. Ryttov and F. Sannino, *Ultra Minimal Technicolor and its Dark Matter TIMP*, *Phys. Rev. D* **78** (2008) 115010 [[0809.0713](#)].
- [52] C. Michael, *Adjoint Sources in Lattice Gauge Theory*, *Nucl. Phys. B* **259** (1985) 58.
- [53] M. Luscher and U. Wolff, *How to Calculate the Elastic Scattering Matrix in Two-dimensional Quantum Field Theories by Numerical Simulation*, *Nucl. Phys. B* **339** (1990) 222.
- [54] B. Blossier, M. Della Morte, G. von Hippel, T. Mendes and R. Sommer, *On the generalized eigenvalue method for energies and matrix elements in lattice field theory*, *JHEP* **04** (2009) 094 [[0902.1265](#)].
- [55] V. Drach, T. Janowski and C. Pica, *Update on SU(2) gauge theory with NF = 2 fundamental flavours*, *EPJ Web Conf.* **175** (2018) 08020 [[1710.07218](#)].